PROCEEDINGS OF SCIENCE

Observation of the Crab Nebula and Galactic Center with the improved HAWC reconstruction algorithm

Sohyoun Yun-Cárcamo[a,*]

[a] *University of Maryland, College Park, USA*

E-mail: yunsoh@umd.edu

The performance of the High Altitude Water Cherenkov Gamma-ray Observatory (HAWC) is mainly shaped by its event reconstruction methodologies, which take as input only the footprint left on the ground by the air shower. We discuss here the revamped reconstruction algorithms, including noise suppression cleaning, a refined core reconstruction method using simulations to fit hit observation, addressing systematic error sources in direction reconstruction, and a new gamma/hadron separation approach based on a more accurate model. As a result, HAWC's angular resolution and gamma/hadron separation reach an improvement of a factor of 2 and 3, respectively, at the highest energies for highly inclined showers and can now observe the Galactic Center at a significance of over 5σ. Furthermore, we verify the overall performance improvement by observing the Crab Nebula as a reference source which we observe at 250σ using 2434 days of data.

38th International Cosmic Ray Conference (ICRC2023)
26 July - 3 August, 2023
Nagoya, Japan

*Speaker

PoS(ICRC2023)697

1. Reconstruction and performance improvements

HAWC has been successfully detecting and reconstructing gamma-ray events since 2015. Previously published results, including the third HAWC catalog [1], were based on the "Pass 4" revision of the event reconstruction algorithm. Here we present a substantial update on HAWC's reconstruction algorithm, referred to as the "Pass 5" revision, which was recently completed and will be used for upcoming analyses.

In our reconstruction process, we analyze the incoming shower angle, deposited energy, and various event characteristics to distinguish between gamma-ray induced showers and hadron-induced showers, relying solely on the collection of hit times and pulse amplitudes, measured in recorded photo-electrons (PEs).

1.1 Effective area

In Figure 1, we show the effective collecting area of the detector, comparing the Pass 4 and Pass 5 revisions as a function of the true energy of the simulated primary gamma ray, for events with reconstructed shower core on the array, passing trigger conditions only. There is approximately 3 to 5 times more effective area at low energies for the range of zenith angles from 0° to 46°, mainly due to the inclusion of small events. In previous results published by HAWC, using Pass 4 analysis, we excluded around 80% of our trigger events to avoid coincident noise hits that could compromise the reconstruction quality, hence, the analyses. The noise-dominated regime coincides with the lower-energy primary gamma rays, which develop smaller air showers and hit fewer PMTs, leaving us with insufficient statistics to reconstruct the shower properly.

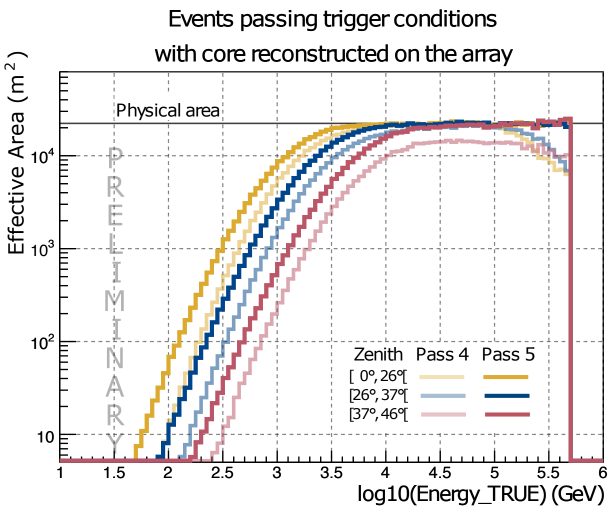

Figure 1: Comparison of the effective area between the Pass 4 (faded light colors) and Pass 5 revisions for three different zenith angle intervals. Events are passing trigger conditions only and with shower cores on the main array. The hard cutoff at $10^{5.7}$ GeV is placed to exclude events that cause saturation of the PMTs in the measured data. With the improvements, the area threshold is lower, and it saturates at the physical area of the detector at the highest energies.

We developed and included in Pass 5 a cleaning algorithm that fits the timing of the hits and assigns them to shower planes. This multi-plane fitter algorithm is applied to the data before the primary reconstruction so that most of the hits that do not belong to showers are already discarded. The hit cleaning algorithm allows the inclusion of showers at low energies that were previously discarded due to high background rate. Despite the poor angular resolution typical of such events, the quality is good enough to be included in analyses.

Moreover, at the highest energies, the effective area improved by over a factor of 2, reaching the detector's physical area in Pass 5 as we are addressing better the saturation of PMT in this energy range.

1.2 Angular resolution

Figure 2 shows the 68% of angular containment as a function of the fraction of PMT hit, which is HAWC's main analysis data binning. Pass 5 includes smaller fractions than Pass 4, as explained in the previous subsection. The angular resolution is determined by the analysis binning by a fraction of PMT hit, with almost no dependence on the zenith angle. The primary enhancement is at the highest zenith angles, reaching an angular 68% of containment around 0.2° at the higher energies. In Pass 5, we identify the core location fitting the lateral distribution to the ones of simulated gamma ray showers in the shower plane instead of the Gaussian approximation in the detector plane used in Pass 4. As a result, we can now distinguish and optimize better the analysis cuts for events whose cores land on or off-array (between the edge of the tank array and a concentric area equal to 1.5 times its size).

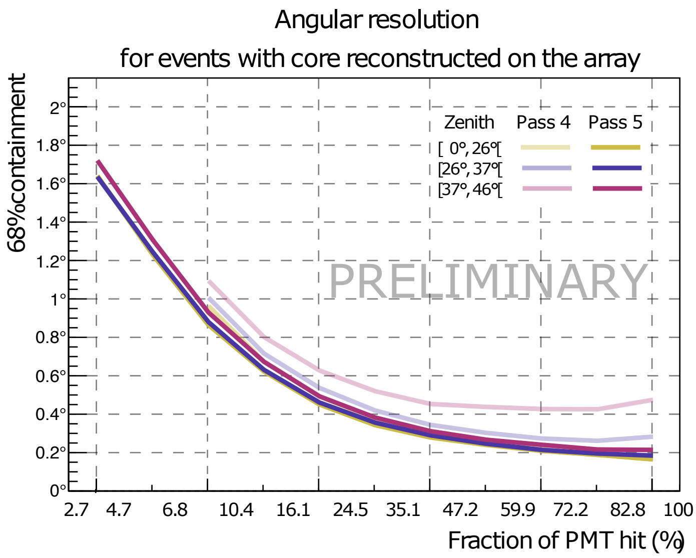

Figure 2: Comparison between the Pass 4 (faded colors) and Pass 5 revision of the angular error with 68% containment. Angular resolution as a function of the fraction of PMTs hit. The main improvement is for showers inclined at large angles and reaching smaller showers (lower energies). Analysis bins determine angular resolution with almost no dependence on the zenith angle in the present revision.

The improvement that had the most impact on the angular resolution performance, though, is the correction of three small but salient systematic errors that mainly affect high zenith angle showers. This corrections include, rectifying the direction of showers off by 0.1° to 0.2°, properly accounting for the tilt of HAWC's main array ground level slope and correcting the shower direction timing hit to the shower plane, not the detector's.

1.3 Gamma/hadron separation

The quality factor (Q) of our gamma/hadron separation cuts is shown in Figure 3, compared to Pass 4. This factor is calculated as

$$Q = \frac{\epsilon_\gamma}{\sqrt{\epsilon_h}}, \tag{1}$$

where ϵ is the fraction of hadrons (data) or gammas (simulations) passing the cuts from the total of events passing trigger conditions. Most of the significant enhancement is for highly inclined showers, with an improvement by a almost factor of 3. For showers hitting more than 25% of the PMTs, the enhancement increases with the shower sizes.

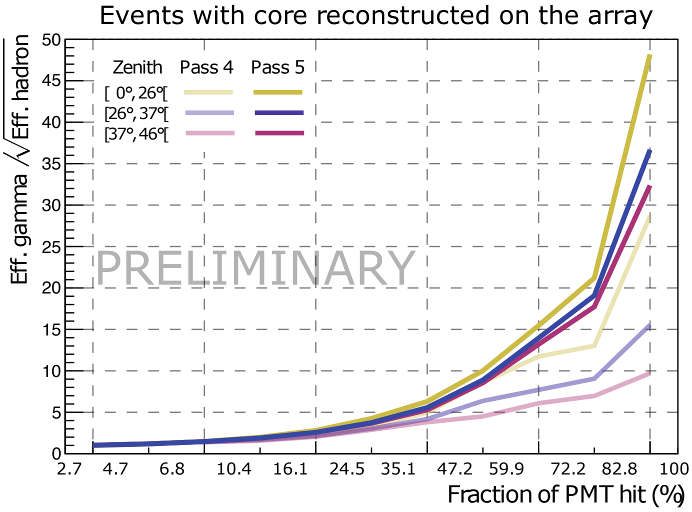

Figure 3: The Q factor as a function of the fraction of PMTs hit in a shower, for Pass 4 (faded colors) and Pass 5 (solid colors).

To achieve these impressive improvements, we replaced a cut based on the identification of nuclear cosmic rays by the reduced χ^2 obtained with one based on fitting the lateral distribution function (LDF) with the NKG function (described in section 2.3 of [2]). This new cut is based on a well-tested model of the radial profile and axial smoothness of gamma-ray showers[3].

2. Verification with the Crab Nebula

We selected events triggering fractions of the total PMTs in three different ranges near the Crab Nebula, which is 3° zenith from HAWC. Using a likelihood framework with a point-like source hypothesis, we obtained a maximum significance of 250 σ during the 2434 days of data. The significance maps for each analysis bin, presented in Figure 4, show maximum significances of 49.1 σ, 101.6 σ, and 62.8 σ, for bins by fraction of PMTs hit with median energies 0.7, 6.0 and 35.0 TeV, respectively. The next subsection illustrates the integrated angular distribution of these high-significance signals.

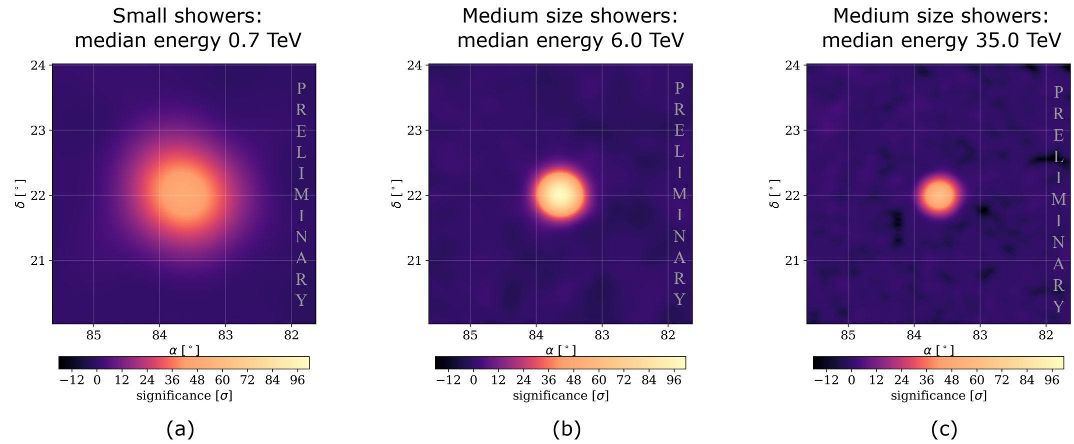

Figure 4: Using 2090 days of data, the Crab Nebula's maximum significances are 49.1 σ, 101.6 σ, and 62.8 σ, respectively. These correspond to 10.4% - 16.1%, 47.2% - 59.9%, and 82.8%-100% fractions of the total PMTs triggered, respectively.

2.1 Angular resolution

The distribution of signal and background events from the Crab Nebula location and vicinity for the three selected bins is shown in Figure 5. It is presented as a function of θ^2, where θ is the measured angular distance to the source. The data was used to verify that the point spread function (PSF) is well simulated for small, medium, and large events, as described in Section 3.3 of [4]. The signal distribution becomes narrower as the shower's size increases, improving the statistics and HAWC's reconstruction performance, which is in line with the simulation performance plots shown in Figure 2. The angular containment at 68% was calculated from the distributions and obtained as 0.61°, 0.24° and 0.19° for small, medium, and large events, respectively.

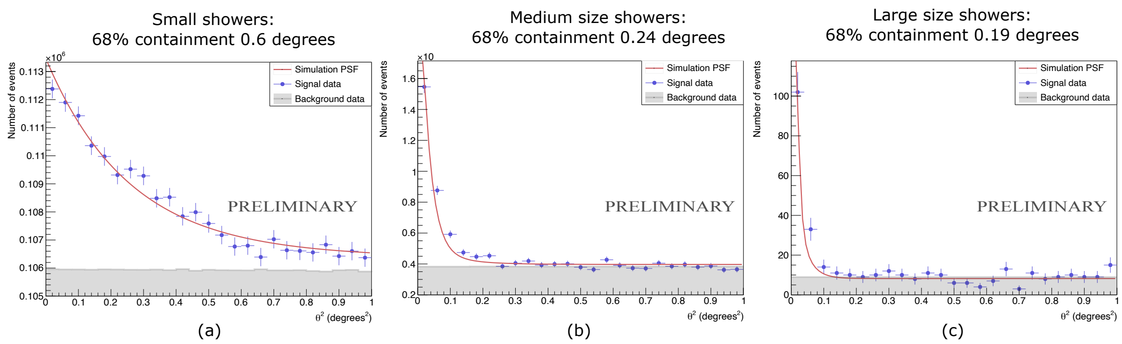

Figure 5: The red line in the figure represents the point spread function fit, while the blue markers indicate signal events and the grey area shows the background data. The fractions of the total PMTs triggered for the three selected bins are 10.4% - 16.1%, 47.2% - 59.9%, and 82.8%-100%, respectively. As the shower size increases, the angular resolution improves due to better statistics and Pass 5 HAWC's reconstruction algorithm. It should be noted that the axes have different scales.

3. Conclusion

The HAWC collaboration has made significant improvements to the reconstruction algorithm, resulting in an enhanced detector performance. Incorporating the MPF algorithm for noise suppression is crucial in analyzing small events that greatly impact the low-energy effective area. This allows for the detection of distant active galaxy nuclei and gamma-ray bursts below 300 GeV[5, 6]. Improving core reconstruction using simulated gamma-ray showers and correcting systematic errors in direction fitting has improved our angular containment for highly inclined showers by a factor of 2 at the highest energies. We have also achieved a factor of 3 improvement in the Q factor in the same regime and can now observe the galactic center at over 5.7σ of significance (see Figure 6). The Pass 5 reconstruction algorithm has been verified through the observation of the Crab Nebula in three different bins (by fraction of PMT hit), with maximum significances of $49.1\,\sigma$, $101.6\,\sigma$, and $62.8\,\sigma$ and median energies of 0.7, 6.0 and 35.0 TeV respectively, over 2434 days. There's an overall agreement between the 68% angular containment from simulations and data.

As a result of these enhancements, HAWC can now detect previously invisible sources above the 5σ significance threshold, and we are preparing an updated source catalog. This advanced reconstruction algorithm also brings us closer to incorporating our outrigger array into the future Pass 6 revision.

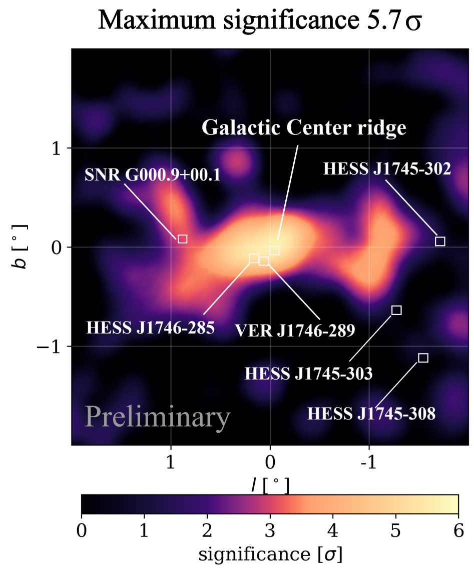

Figure 6: Preliminary significance map of the Galactic Center region using all the bins from our analysis by fraction of PMT hit. The maximum significance detected in this region is $5.7\,\sigma$.

References

[1] Albert, A., et al. "3HWC: The third HAWC catalog of very-high-energy gamma-ray sources." The Astrophysical Journal 905.1 (2020): 76.

[2] Alfaro, R., Alvarez, C., Álvarez, J., et al. 2022, preprint arXiv:2205.12188

[3] Krawczynski, H., Carter-Lewis, D., Duke, C., et al. 2006,418 Astroparticle Physics, 25, 380

[4] Abeysekara, A., Albert, A., Alfaro, R., et al. 2017b, The Astrophysical Journal, 843, 39376

[5] Yuan, C., Murase, K., Guetta, D., et al. 2022, The Astrophysical Journal, 932, 80

[6] Biteau, J., Meyer, M. 2022, Galaxies, 10, doi: doi.org/10.3390/galaxies10020039

4. Acknowledgements

We acknowledge the support from: the US National Science Foundation (NSF); the US Department of Energy Office of High-Energy Physics; the Laboratory Directed Research and Development (LDRD) program of Los Alamos National Laboratory; Consejo Nacional de Ciencia y Tecnología (CONACyT), México, grants 271051, 232656, 260378, 179588, 254964, 258865, 243290, 132197, A1-S-46288, A1-S-22784, CF-2023-I-645, cátedras 873, 1563, 341, 323, Red HAWC, México; DGAPA-UNAM grants IG101323, IN111716-3, IN111419, IA102019, IN106521, IN110621, IN110521 , IN102223; VIEP-BUAP; PIFI 2012, 2013, PROFOCIE 2014, 2015; the University of Wisconsin Alumni Research Foundation; the Institute of Geophysics, Planetary Physics, and Signatures at Los Alamos National Laboratory; Polish Science Centre grant, DEC-2017/27/B/ST9/02272; Coordinación de la Investigación Científica de la Universidad Michoacana; Royal Society - Newton Advanced Fellowship 180385; Generalitat Valenciana, grant CIDEGENT/2018/034; The Program Management Unit for Human Resources & Institutional Development, Research and Innovation, NXPO (grant number B16F630069); Coordinación General Académica e Innovación (CGAI-UdeG), PRODEP-SEP UDG-CA-499; Institute of Cosmic Ray Research (ICRR), University of Tokyo. H.F. acknowledges support by NASA under award number 80GSFC21M0002. We also acknowledge the significant contributions over many years of Stefan Westerhoff, Gaurang Yodh and Arnulfo Zepeda Dominguez, all deceased members of the HAWC collaboration. Thanks to Scott Delay, Luciano Díaz and Eduardo Murrieta for technical support.

Full Authors List: Collaboration

A. Albert[1], R. Alfaro[2], C. Alvarez[3], A. Andrés[4], J.C. Arteaga-Velázquez[5], D. Avila Rojas[2], H.A. Ayala Solares[6], R. Babu[7], E. Belmont-Moreno[2], K.S. Caballero-Mora[3], T. Capistrán[4], S. Yun-Cárcamo[8], A. Carramiñana[9], F. Carreón[4], U. Cotti[5], J. Cotzomi[26], S. Coutiño de León[10], E. De la Fuente[11], D. Depaoli[12], C. de León[5], R. Diaz Hernandez[9], J.C. Díaz-Vélez[11], B.L. Dingus[1], M. Durocher[1], M.A. DuVernois[10], K. Engel[8], C. Espinoza[2], K.L. Fan[8], K. Fang[10], N.I. Fraija[4], J.A. García-González[13], F. Garfias[4], H. Goksu[12], M.M. González[4], J.A. Goodman[8], S. Groetsch[7], J.P. Harding[1], S. Hernandez[2], I. Herzog[14], J. Hinton[12], D. Huang[7], F. Hueyotl-Zahuantitla[3], P. Hüntemeyer[7], A. Iriarte[4], V. Joshi[28], S. Kaufmann[15], D. Kieda[16], A. Lara[17], J. Lee[18], W.H. Lee[4], H. León Vargas[2], J. Linnemann[14], A.L. Longinotti[4], G. Luis-Raya[15], K. Malone[19], J. Martínez-Castro[20], J.A.J. Matthews[21], P. Miranda-Romagnoli[22], J. Montes[4], J.A. Morales-Soto[5], M. Mostafá[6], L. Nellen[23], M.U. Nisa[14], R. Noriega-Papaqui[22], L. Olivera-Nieto[12], N. Omodei[24], Y. Pérez Araujo[4], E.G. Pérez-Pérez[15], A. Pratts[2], C.D. Rho[25], D. Rosa-Gonzalez[9], E. Ruiz-Velasco[12], H. Salazar[26], D. Salazar-Gallegos[14], A. Sandoval[2], M. Schneider[8], G. Schwefer[12], J. Serna-Franco[2], A.J. Smith[8], Y. Son[18], R.W. Springer[16], O. Tibolla[15], K. Tollefson[14], I. Torres[9], R. Torres-Escobedo[27], R. Turner[7], F. Ureña-Mena[9], E. Varela[26], L. Villaseñor[26], X. Wang[7], I.J. Watson[18], F. Werner[12], K. Whitaker[6], E. Willox[8], H. Wu[10], H. Zhou[27]

[1]Physics Division, Los Alamos National Laboratory, Los Alamos, NM, USA, [2]Instituto de Física, Universidad Nacional Autónoma de México, Ciudad de México, México, [3]Universidad Autónoma de Chiapas, Tuxtla Gutiérrez, Chiapas, México, [4]Instituto de Astronomía, Universidad Nacional Autónoma de México, Ciudad de México, México, [5]Instituto de Física y Matemáticas, Universidad Michoacana de San Nicolás de Hidalgo, Morelia, Michoacán, México, [6]Department of Physics, Pennsylvania State University, University Park, PA, USA, [7]Department of Physics, Michigan Technological University, Houghton, MI, USA, [8]Department of Physics, University of Maryland, College Park, MD, USA, [9]Instituto Nacional de Astrofísica, Óptica y Electrónica, Tonantzintla, Puebla, México, [10]Department of Physics, University of Wisconsin-Madison, Madison, WI, USA, [11]CUCEI, CUCEA, Universidad de Guadalajara, Guadalajara, Jalisco, México, [12]Max-Planck Institute for Nuclear Physics, Heidelberg, Germany, [13]Tecnologico de Monterrey, Escuela de Ingeniería y Ciencias, Ave. Eugenio Garza Sada 2501, Monterrey, N.L., 64849, México, [14]Department of Physics and Astronomy, Michigan State University, East Lansing, MI, USA, [15]Universidad Politécnica de Pachuca, Pachuca, Hgo, México, [16]Department of Physics and Astronomy, University of Utah, Salt Lake City, UT, USA, [17]Instituto de Geofísica, Universidad Nacional Autónoma de México, Ciudad de México, México, [18]University of Seoul, Seoul, Rep. of Korea, [19]Space Science and Applications Group, Los Alamos National Laboratory, Los Alamos, NM USA [20]Centro de Investigación en Computación, Instituto Politécnico Nacional, Ciudad de México, México, [21]Department of Physics and Astronomy, University of New Mexico, Albuquerque, NM, USA, [22]Universidad Autónoma del Estado de Hidalgo, Pachuca, Hgo., México, [23]Instituto de Ciencias Nucleares, Universidad Nacional Autónoma de México, Ciudad de México, México, [24]Stanford University, Stanford, CA, USA, [25]Department of Physics, Sungkyunkwan University, Suwon, South Korea, [26]Facultad de Ciencias Físico Matemáticas, Benemérita Universidad Autónoma de Puebla, Puebla, México, [27]Tsung-Dao Lee Institute and School of Physics and Astronomy, Shanghai Jiao Tong University, Shanghai, China, [28]Erlangen Centre for Astroparticle Physics, Friedrich Alexander Universität, Erlangen, BY, Germany

PoS(ICRC2023)697